Biomimetic Chemistry of Iron, Nickel, Molybdenum, and Tungsten in Sulfur−Ligated Protein Sites

ARTICLE *in* BIOCHEMISTRY · MARCH 2009

Impact Factor: 3.02 · DOI: 10.1021/bi900044e · Source: PubMed

Published in final edited form as:
Biochemistry. 2009 March 24; 48(11): 2310–2320. doi:10.1021/bi900044e.

Biomimetic Chemistry of Iron, Nickel, Molybdenum, and Tungsten in Sulfur-Ligated Protein Sites†

Stanislav Groysman and **R. H. Holm***
Department of Chemistry and Chemical Biology, Harvard University, Cambridge, Massachusetts 02138

Abstract

Biomimetic inorganic chemistry has as its primary goal the synthesis of molecules that approach or achieve the structures, oxidation states, and electronic and reactivity features of native metal-containing sites of variant nuclearity. Comparison of properties of accurate analogues and these sites ideally provides insight into the influence of protein structure and environment on intrinsic properties as represented by the analogue. For polynuclear sites in particular, the goal provides a formidable challenge for, with the exception of iron-sulfur clusters, all such site structures have never been achieved and few even closely approximated by chemical synthesis. This account describes the current status of the synthetic analogue approach as applied to the mononuclear sites in certain molybdoenzymes and the polynuclear sites in hydrogenases, nitrogenase, and carbon monoxide dehydrogenases.

Synthetic Analogues

A strategy of demonstrated value in the study of protein-bound metal sites is the *synthetic analogue* or biomimetic approach defined by the protocol of Figure 1 (1). As developed and implemented in this laboratory, this approach has as its objective the preparation and detailed characterization of relatively small molecules that simulate or achieve the coordination sphere, composition, stereochemistry, and oxidation states of the native metal mononuclear or polynuclear site. A *structural* analogue allows deduction of site characteristics common to the site and itself by property comparisons. A *functional* analogue supports substrate transformations to products as do enzymes, although not necessarily at the same rate or with the same stereochemistry. A functional analogue is not inevitably a structural analogue, but a high-fidelity structural analogue should be a functional analogue provided a protein environment is not obligatory to reactivity. The approach is iterative in order to improve as necessary the accuracy of a site analogue. Here we describe the current status of selected biomimetic chemistry of four metals (Fe, Ni, Mo, W) in relation to proteins that are the objects of widespread contemporary interest: molybdenum and tungsten oxotransferases and hydroxylases, iron and nickel-iron hydrogenases, iron-sulfur proteins, molybdenum-copper and nickel-iron-sulfur carbon monoxide dehydrogenases, and nitrogenase. The sites in these proteins exhibit a range of metal nuclearities and have the common features of variable oxidation states and sulfur-rich coordination environments. Space limitations do not allow detailed accounts of enzyme reactions and mechanisms, protein structure, and inclusion of all meritorious results in site modeling. The emphasis is on the native sites themselves and recent

†Research in this laboratory is supported by NIH Grant GM 28856 and NSF Grant CHE 00547734.

*To whom correspondence should be addressed: holm@chemisty.harvard.edu; Department of Chemistry and Chemical Biology, Harvard University, 12 Oxford Street, Cambridge, MA 02138, phone (617) 495-0853, fax (617) 496-9289.

synthetic inorganic chemistry directed toward meaningful analogues of those sites. More extensive accounts of the biomimetic chemistry of protein sites are available (2,3).

Molybdenum/Tungsten Oxotransferases and Hydroxylases

These enzymes catalyze overall reaction [1] in which generalized substrate X/XO is converted to product XO/X by addition or removal of one oxygen atom whose ultimate source is water (4-7). Current interpretation of function derives substantially from more than thirty crystal

$$X+H_2O \leftrightarrow XO+2H^+ +2e^- \quad [1]$$

structures of enzymes that catalyze over a dozen different reactions. Molybdoenzymes are effectively organized under the Hille classification, which is partly based on the structures of oxidized (Mo^{VI}) active sites and includes the DMSOR,[1] SO, and XOR families (4). Active site structures in the DMSOR family (Figure 2) contain two pyranopterindithiolate(2-) cofactor ligands as in distorted trigonal prismatic $\{Mo^{VI}O(L)(S_2pd)_2\}$ with L = O_{Ser} (**1**, DMSOR) (8), S_{Cys} (**2**, dissimilatory NiR) (9), and Se_{Cys} (**3**, FDH) (10,11). Although FDH catalyzes the process $HCO_2 \leftrightarrow CO_2 + H^+ + 2e^-$ and not reaction [1], it is placed in the DMSOR family because of site structural similarity. Also shown are the tungstoenzyme sites $\{W^{IV}(OH_2)(S_{Cys})(S_2pd)_2\}$ of acetylene hydratase (**4**) (12) and $\{W^{VI}(SH)(Se_{Cys})(S_2pd)_2\}$ of FDH (**5**) (13). Sites in the SO and XOR families contain one cofactor ligand (Figure 3) and include the oxidized sites $\{MoO_2(S_{Cys})(S_2pd)\}$ of chicken liver and plant SO (**6**) (14,15), $\{MoO_2S(S_2pd)\}$ of quinoline 2-oxidoreductase (**7**) (16), and a substrate complex of the milk XOR site (**8**) (17). The wealth of structural information from crystallography and X-ray absorption spectroscopy is the single most important factor leading to the development of active site analogues. The cofactor ligand functions in the ene-1,2-dithiolate form (Figure 2), the terminal reduced member of the dithiolene class of prototypical non-innocent ligands that encompasses the oxidation states $(R_2C_2S_2)^{2-,1-,0}$ (18). Biomimetic research focuses on the chemistry of mononuclear complexes in the physiological oxidation states $M^{IV,V,VI}$.

Of the many non-dithiolene ligand platforms employed, several have proven especially useful (Figure 4). Complexes of tridentate hydrotris(pyrazolyl)borate **9** with variable substituents R have been valuable in disclosing fundamental properties of molybdenum and tungsten in physiological oxidation states (19,20), albeit not in coordination environments closely similar to enzyme sites. As examples, species such as **10** execute the minimal oxygen atom transfer reaction [2] with disclosure of mechanistic details (21), and support proton-coupled electron transfer reactions and a catalytic cycle (22) that parallels the enzymatic cycle; another variant sustains the uncommon *cis*-$Mo^{VI}OS$ fragment (23) found in the XOR family. Bidentate ligand **11** illustrates the concept of steric suppression of nonphysiological reaction [3], allowing reaction 2 with components **12** and **13** and

$$Mo^{IV}O+XO \leftrightarrow Mo^{VI}O_2+X \quad [2]$$

$$Mo^{IV}O+Mo^{VI}O_2 \leftrightarrow OMo^{V}-O-Mo^{V}O \quad [3]$$

a wide variety of substrates to proceed without complication (24). Dithiolate ligands **14** closely simulate the structural and electronic features imposed by the cofactor ligand. Three common

and useful types are shown, of which **14a** is most like the natural ligand. Substituent variation alters electron density at the sulfur atoms and modulates redox potentials.

Structural Analogues

Efficient syntheses afford analogues of reduced (desoxo Mo^{IV}) and oxidized (monooxo Mo^{VI}) sites in the DMSOR family (Figure 5) (20,25-28). The mdt ligand has not been isolated as a stable salt but is accessible by the indicated ligand transfer reaction to form the M = Mo/W dicarbonyl complexes **15**. The labile carbonyl groups are displaced to yield the terminal oxo/sulfido complexes **16**, the η^2-carboxylates **17**, and square pyramidal species **18**, which are also obtainable from **17** with silylthio or silylseleno reagants. To assure stable mononuclear structures, complexes **18** are prepared with sterically bulky R-substituents. The scheme is completed by oxo transfer reactions with XO = Me_3NO or Ph_3AsO to give monooxo complexes **19** and by a sulfur atom transfer reaction to afford **20**. These complexes can be isolated only with tungsten. As is the case here, Mo^{VI} complexes are often unstable to autoreduction in anionic sulfur ligand environments. Because isoligated complexes of Mo^{VI}/W^{VI} are always isostructural and practically isometric, the approach has afforded structural analogues **19** of three oxidized sites in the DMSOR family and one analogue **20** of a tungstoenzyme site (compare Figure 2). Further, complexes **18** are analogues of reduced sites, **17** (M = Mo) is a representative of the site of a membrane-bound NiR of *E. coli* (29), and Mo=S complex **16** models the formate-reduced site in a reinterpretation of the mechanism of *E. coli* FDH_H (30). Analogue complexes are unprotonated versions with M=Q rather than the M-QH groups often found in enzyme sites.

Structural analogues of oxidized sites of the SO and XOR families have been synthesized utilizing dithiolate **14c** (Figure 6). A sequence of substitution reactions yields **21**, an analogue of the SO site in which an hindered thiolate simulates conserved cysteinate in site **6** (31). In seeking XOR site analogues, W^{VI} complexes have again been used because of the redox instability of Mo^{VI}. Removal of oxo ligands as siloxane from tungstate precursors leads to **22**, an analogue of an oxidized inactive site, and **23**, an analogue of the site in oxidized active enzymes (32). Native sites are often protonated, a condition simulated for structural purposes by silylation to give **24** and **25**. Protonated species have not yet been isolated. Complex **23** is a long-sought structural analogue with a single basal sulfido ligand, as in native site **7**, a position maintained upon reduction by substrate to the (probable) Mo^{IV} state in **8**.

Accurate analogues present structures unmodified by a protein environment. Superposition of analogue (**19, 21-25**) and oxidized protein site structures reveal near-congruency in most cases, with weighted rms deviations in atom positions of ≤0.30 Å (31-33). Protein interactions evidently do not cause major perturbations of intrinsic structures as represented by analogue complexes in their crystal lattices.

Functional Analogues

Certain of the preceding complexes manifest reductase activity with biological substrates (Figure 7). Complexes **18** cleanly reduce substrate in atom transfer reactions analogous to those of DMSOR and trimethylamine *N*-oxide, nitrate, and selenate reductases (20,27,28), albeit at much slower rates. The $Mo^{VI}O$ analogues of **19** were generated as reaction products but not isolated. Reactions are second order with associative transition states; activation parameters for the reduction of $(CH_2)_4SO$ by $[Mo(OPh)(mdt)_2]^{1-}$ in acetonitrile ($k_2^{298} = 1.5 \times 10^4$ $M^{-1}s^{-1}$) are typical: $\Delta H^{\ddagger} = 10$ kcal/mol, $\Delta S^{\ddagger} = -39$ eu. These reactions exhibit a small kinetic metal effect, $k_2^W/k_2^{Mo} \approx 6\text{-}30$, in the reduction of constant substrate. A related effect observed with molybdenum and tungsten isoenzymes is intrinsic to the metals, and is associated with the periodic behavior of isostructural and isoelectronic couples of the two metals. These reactions simulate the oxo atom transfer step in a single turnover of an enzyme. In a functional

NiR analogue system, oxo transfer reaction [5] is coupled to equilibrium reaction [4] in dichloromethane with the result that Michaelis-Menton saturation kinetics are followed (34).

$$[Mo^{IV}(SR)(PPh_3)(mnt)_2]^{1-} \leftrightarrow [Mo^{IV}(SR)(mnt)_2]^{1-} + PPh_3 \quad [4]$$

$$[Mo^{IV}(SR)(mnt)_2]^{1-} + NO_3^- \rightarrow [Mo^{VI}O(SR)(mnt)_2]^{1-} + NO_2^- \quad [5]$$

Molybdenum and tungsten dithiolene complexes form the basis for systems in which both accurate structural *and* suitably functional analogues have been realized, an ultimate but infrequently achieved goal in synthetic analogue chemistry. Functional analogues refer to *oxotransferases* that are reductases. However, the picture will remain incomplete pending the development of oxidase analogue systems. One such system has been briefly described in relation to arsenite oxidase (35). As yet there are no effective systems for substrates of the XOR family. These enzymes are *hydroxylases* that utilize Mo^{VI}-OH units as base-activated nucleophiles in the reaction pathway rather than metal sites as oxygen atom donors or acceptors (6).

Hydrogenases

Hydrogenases occur in bacteria, archaea, and eukarya and catalyze bidirectional reaction [6]. They consist of two main classes, the [NiFe] (36,37) and [FeFe] (37-39) hydrogenases, so designated because of their active site metal content. A subgroup of the first class is the [NiFeSe] hydrogenases which contain a selenocysteinate in place of a cysteinate ligand. A third class, [Fe] hydrogenases,

$$H_2 \leftrightarrow 2H^+ + 2e^- \quad [6]$$

contain mononuclear sites (40) and is not considered here. Synthetic approaches to [NiFe] and [FeFe] enzyme sites require construction of binuclear species and in the latter case, attachment to an Fe_4S_4 cubane-type cluster. The binuclear site and site fragment structures project an apparent attainability, which together with the importance of the problem, has resulted in extensive activity in site modeling, many aspects of which have been summarized (41-45). We truncate the subject to a small set of attractive developments.

[NiFe] Hydrogenases

A combination of X-ray crystallographic and FTIR studies has led to the formulations **26a** for the oxidized site and **27a** for the reduced site (Figure 8) (36,37,46,47). For each, a specific structure **26b** (48) or **27b** (49) is provided. In the oxidized site, X is a generalized bridging ligand, thought to be an oxygenic species as indicated by O in **26b**, while in the reduced site the bridging position is vacant or perhaps occupied by hydride. Appropriate initial analogues are heterometal binuclear species containing the $(RS)_2Ni^{II}(\mu_2\text{-}SR)_2Fe^{II}$ fragment with Ni-Fe separations of 2.5-2.9 Å and distorted octahedral low-spin Fe^{II} coordinated to one carbonyl and two cyanide ligands. A significant portion of synthetic research has focused on mononuclear iron or nickel sites (Figure 9). Among sulfur-ligated species, **28** reproduces Fe $(CN)_2(CO)$ coordination at the low-spin Fe^{II} site (50), **29** evolves dihydrogen from HCl nearly quantitatively in the overall reaction $Ni^I + H^+ \rightarrow Ni^{II} + ½\ H_2$ (51), and **30** catalyzes D_2/H^+ exchange consistent with enzymatic heterolytic cleavage of D_2 or H_2 (52). A variety of

dinuclear Ni-Fe complexes are accessible by reactions of suitable mononuclear components, as in the formation of **31** (53). This molecule illustrates the feasibility of the $Ni^{II}(\mu_2\text{-}SR)_2Fe^{II}$ bridge fragment, low-spin Fe^{II} in the unit $Fe(SR)_2(CN)_2(CO)_2$, and a Ni···Fe separation near the upper end found in enzyme sites. Complex **32** reveals stabilization of low-spin Fe^{II} in a site containing three strong field ligands, and contains a similar bridge fragment with exclusive sulfur coordination at Ni^{II} but a considerably longer Ni···Fe distance (3.29 Å) (54). No functional dinuclear NiFe analogues have yet been devised. However, in a variation on a native metal, the $Fe^{II}(CN)_2(CO)$ unit was replaced by isoelectronic $(C_6Me_6)Ru^{II}$ to give a complex with the bridge $Ni^{II}(\mu_2\text{-}SR)_2Ru^{II}$ incorporating a metal that forms stable dihydrogen complexes. The complex reacts with dihydrogen in water, affording a structurally related dinuclear product augmented with the hydride bridge $Ni^{II}(\mu_2\text{-}H)Ru^{II}$ and protons released in solution (55). A plausible intermediate in the enzymatic uptake of H_2 is site **27a** with hydride occupying the vacant bridge position.

[FeFe] Hydrogenases

The active sites of these enzymes are termed *H-clusters* and exist in three oxidation levels, air-oxidized inactive ($Fe^{II}Fe^{II}$), oxidized-active ($Fe^{II}Fe^{I}$), and reduced-active ($Fe^{I}Fe^{I}$) with proposed oxidation states indicated. The structure of an oxidized-active site **33** (Figure 10) (56) reveals a dinuclear $Fe_2(\mu_2\text{-}CO)(\mu_2\text{-}SR)_2(CO)_2(CN)$ fragment containing the dithiolate SCH_2XCH_2S (in which atom/group X = CH_2, NH, or O is not definitely identified) linked by an $Fe(\mu_2\text{-}S_{Cys})Fe$ bridge to an Fe_4S_4 cluster. The iron sites are six-coordinate and that distal to the cysteinate bridge contains an aquo ligand. The problem reduces to synthesis of a suitable dinuclear fragment and attachment through an unsupported bridge to the Fe_4S_4 cluster.

Approaches to the dinuclear fragment often begin with the Seyferth anion $[Fe^{I}_2S_2(CO)_6]^{2-}$, which is readily dialkylated to $[Fe_2(SR)_2(CO)_6]$ (57), thereby generating a core structure closely related to that in **33**. Structures with variable X and substitution of cyanide or tertiary phosphine for carbonyl have been achieved in extensive modeling studies (41,43). Carbon monoxide, cyanide, and phosphine have the common properties of π-acid behavior and stabilization of low oxidation states. In one example of structural modeling (Figure 11), dithiolate cluster **34** undergoes CO substitution to place the phosphines in **35** at the positions of cyanide in **33**, followed by oxidation to yield the $Fe^{II}Fe^{I}$ product **36** with an asymmetric carbonyl bridge (58). An approach to the entire H-cluster framework is represented by the reaction of 1:3 subsite-differentiated cluster **37** (59) with functionalized **38** to afford a product whose physicochemical properties have been interpreted in terms of the assembly **39** in which cluster and dinuclear unit are linked by an unsupported $Fe(\mu_2\text{-}SR)Fe$ bridge (60). The viability of the structure is supported by DFT calculations which indicate the $Fe^{I}Fe^{I}$ and $[Fe_4S_4]^{2+}$ oxidation levels. The H-cluster model and certain dinuclear species are catalysts for electrochemical dihydrogen evolution at strongly reducing potentials (61) while another $Fe^{I}Fe^{I}$ complex activates dihydrogen photochemically in the form of an $Fe^{II}Fe^{II}$ dihydride (62).

Iron-Sulfur Proteins

These proteins are of widespread occurrence at all levels of life and are implicated in electron transfer and other multifarious functions (63,64). Clusters with rhomboidal Fe_2S_2 (**40,41**) (65,66), cuboidal Fe_3S_4 (**42**) (67), and cubane-type Fe_4S_4 (**43**) (68) cores (Figure 12) are ubiquitous and exist in at least two oxidation states necessary for redox behavior. Analogues of the **40**, **43**, and the $\{Fe(S_{Cys})_4\}$ site in rubredoxins (not shown) were prepared at the very beginning of biomimetic inorganic chemistry, and were followed later by an analogue of **42**. Different core oxidation states are achieved by appropriate choice of $Fe^{II,III}$ reactants in synthesis or by redox reactions of isolated clusters. The development and accomplishments of iron-sulfur analogue chemistry and a summary of synthetic methods affording iron-sulfur

clusters are available (69,70). In analogue clusters, terminal cysteinate ligation is a simulated by organic thiolates. Despite the advanced state of iron-sulfur analogue chemistry, several problems, including the complicated clusters of nitrogenase and carbon monoxide dehydrogenase (vide infra) remain, while progress has been made on two others, the Rieske cluster and the fully reduced Fe_4S_4 cluster of the Fe protein of nitrogenase.

Rieske proteins function in electron transport and contain cluster **41**, differentiated from the more common Fe_2S_2 cluster **40** by the presence of two Im_{His} ligands (71). Reaction of $[Fe_2S_2Cl_4]^{2-}$ with *o*-xylyldithiolate and the dilithium salt of 2,2′-bis(methylindolyl) phenylmethane affords the $Fe^{III}Fe^{III}$ complex **44** (Figure 13), having the same ligation pattern as **41** (72). It undergoes a reversible one-electron reduction at a potential *ca.* 150 mV less negative than $[Fe_2S_2(S_2\text{-}o\text{-}xyl)_2]^{2-}$, an accurate analogue of **40**, and exhibits a rhombic EPR spectrum similar to that of a reduced ($Fe^{III}Fe^{II}$) Rieske center. Potentials of proteins with cluster **40** are more negative than those of Rieske proteins, which encompass the range -150 to +400 mV vs. SHE, a variability largely due to electrostatic effects (73). Reduction of **44** apparently occurs at the FeN_2S_2 site, as for Rieske centers. Although this cluster is not an exact analogue of a Rieske cluster owing to binding of two anionic nitrogen ligands rather than neutral imidazoles, it is the closest approach yet to the native cluster itself.

Cubane-type clusters **43** are the most widely dispersed of all iron-sulfur species and are well known in proteins and analogue molecules in the electronically delocalized core oxidation states 3+, 2+, and 1+ of redox series [7] in which adjacent members are interconverted by one-electron transfer. The proposal that the Fe protein of nitrogenase might utilize the $[Fe_4S_4]^{2+/1+;1+/0}$ couples in delivering electrons to the catalytic site of nitrogenase was followed by definite proof of the existence of the $[Fe_4S_4]^0$ oxidation state in the fully reduced Fe protein (74,75). These results render an isolable

$$\begin{array}{cccccc} [Fe_4S_4]^0 & \leftrightarrow & [Fe_4S_4]^{1+} & \leftrightarrow & [Fe_4S_4]^{2+} & \leftrightarrow & [Fe_4S_4]^{3+} \\ 4Fe^{2+} & & 3Fe^{2+}+Fe^{3+} & & 2Fe^{2+}+2Fe^{3+} & & Fe^{2+}+3Fe^{3+} \end{array} \quad [7]$$

all-ferrous analogue a significant objective. The first such species was isolated from the substitution reaction of $[Fe_4S_4(PPr^i_3)_4]^{1+}$ with cyanide in the presence of the strong reductant $[Ph_2CO]^{\bullet -}$ (76). However, $[Fe_4S_4(CN)_4]^{4-}$, while in the desired oxidation state, was intensely unstable to oxidation and difficult to manipulate. Use of a *N*-heterocyclic carbene as a strong σ-donor terminal ligand in a cluster assembly system with an Fe^{II} reactant and a soluble sulfide source leads to cluster **45** (Figure 13) (77), which is amenable to study. Its ^{57}Fe isomer shift and comparative structural parameters are fully consistent with an all-ferrous formulation. Further, the magnetic Mössbauer and integer spin EPR spectra of **45** disclose the unusual spin ground state $S = 4$ (78), also found for the fully reduced native Fe protein (74) where it is unique in biology. The synthetic cluster is a meaningful analogue of the protein-bound $[Fe_4S_4]^0$ cluster, providing further evidence that magnetic properties arise from interactions within the core and are not strongly influenced by terminal ligation (here S_{Cys} vs. C). The two all-ferrous clusters complete the synthesis of isolable analogues of all known biological oxidation states of Fe_4S_4 clusters.

Carbon Monoxide Dehydrogenases

These enzymes occur in aerobic and anaerobic bacteria and archaea and catalyze the reversible interconversion of carbon monoxide and carbon dioxide in reaction [8] at two very different types of catalytic sites. Cu-Mo CODH occurs in aerobic organisms (79) while Ni-Fe CODHs are found in anaerobic organisms (80-82). The enzymes are highly significant agents in global carbon cycling. Synthetic analogue chemistry of their catalytic sites is at an early stage.

$$CO+H_2O \leftrightarrow CO_2+2H^+ +2e^- \quad [8]$$

Mo-Cu CODH

The oxidized site **46** (Mo^{VI}/Cu^{I}, Figure 14) (83) resembles site **7** in the XOR family (Figure 3) with the inclusion of a Cu^{I}-S_{Cys} fragment bound to the basal sulfido ligand. Two synthetic approaches to the site have emerged (Figure 15). Reaction of a Cu^{I} triazamacrocyclic complex with a six-coordinate $Mo^{V}OS$ complex **47** results in displacement of acetonitrile and formation of assembly **48** (84). This species establishes the synthetic viability of an unsupported Mo^{V}-S-Cu^{I} bridge based on an initially terminal sulfido ligand; metric features (Mo-S 2.284 Å, Cu-S 2.135 Å, Mo-S-Cu 118.9 °, Mo···Cu 3.74 Å) resemble those of site **46**. Further, EPR spectra and DFT calculations establish that unpaired electron density extends to the Cu^{I} site. While this complex lacks dithiolate binding simulating the cofactor ligand, it provides another example of the utility of the hydrotris(pyrazolyl)borate ligand platform in stabilizing a structural element of a molybdoenzyme site. A second relevant reaction affords the square pyramidal Mo^{VI} complex **49** that incorporates the enzyme site features of an apical oxo atom, basal dithiolate coordination, and basal sulfido coordination to Cu^{I} (85). However, it departs from **46** with two sulfido ligands which form mutually supported bridges to Cu^{I}. Complexes **23** and **25** (Figure 6) offer the possibility of a single basal sulfido bridge in square pyramidal coordination as in **46** but with a non-native metal. The reactivity of these species with Cu^{I} is currently under investigation in this laboratory.

Ni-Fe CODH

Structures of the catalytic sites, termed *C-clusters* and depicted generally by **50** which subsumes actual structures **51** and **52** (Figure 16), have the common features of a cubanoid $NiFe_3S_4$ core with an approximately planar nickel site and a tetrahedral Fe^{II} site bridged to the core by atom/group X and a μ_3-S atom. Construction of a site analogue can be proposed in two steps: synthesis of the $NiFe_3S_4$ core containing planar Ni^{II}, followed by binding of Fe^{II} to the cluster through the μ_2-S atom axial to Ni^{II} and a Ni-X-Fe bridge. The conversion of previously prepared cubane-type cluster **53** (86) to **54** and **55** by substitution with strong-field in-plane ligands involves spin-pairing with a concomitant tetrahedral ($S = 1$) → planar ($S = 0$) Ni^{II} structural change and creation of a μ_2-S atom axial to the nickel site (Figure 17) (86, 87). This accomplishes the first step. The structure of the C-cluster of CODH from *C. hydrogenoformans* (1.1 Å resolution) was interpreted in terms of an X = S bridge (89), prompting the introduction of a dithiolate ligand in **55** which might sustain a sulfur bridge to external Fe^{II}. More recently, the crystal structure of recombinant CODH maintained at fixed redox potentials revealed C-clusters of the same overall structure but with X = OH/OH_2 in **51** and X = CO_2 in **52** (Figure 16) after treatment with $NaHCO_3$ at a lower potential (90). This and other evidence indicates that the bridge in the active enzyme does not contain sulfide. The central feature of a structure-based mechanism involves nucleophilic attack by an Fe^{II}-OH group on the carbon atom in Ni^{II}-CO. The bridge unit Ni^{II}-OH/OH_2-Fe^{II} is unknown in any synthetic species. Consequently, the second step in creating a C-cluster remains a formidable challenge.

Nitrogenase

The nitrogenase complex catalyzes the six-electron reduction reaction [9] with simultaneous dihydrogen evolution, and consists of an α_2-Fe protein with an Fe_4S_4 cluster bound between subunits and an $\alpha_2\beta_2$-MoFe protein containing two clusters in each αβ subunit (91,92). The P-cluster is

$$N_2+6H^++6e^- \rightarrow 2NH_3 \quad [9]$$

located at the αβ interface and the cofactor cluster FeMoco is placed within the α subunit. The path of electron flow is most likely Fe_4S_4 → P-cluster → FeMoco; the substrate is bound and reduced at the cofactor cluster by a pathway yet to be defined. Synthetic attempts directed at the P-cluster (**56**) and FeMoco (**57**) (Figure 18) (93-95), the two most complicated and synthetically formidable metalloclusters in biology, commenced well before 1992 when the first crystallographic results at atomic resolution became available. The topological relationship between the two clusters is evident from comparison **58**. The P-cluster contains a μ_6-S *interior* atom within a $Fe_6(\mu_2\text{-}S_{Cys})_2$ cavity and FeMoco an *interstitial* μ_6-X atom (X = C, N, O) (95) within a $Fe_6(\mu_2\text{-}S)_3$ cage. We describe here certain encouraging developments. More extensive accounts of work in this laboratory are available (96,97).

Biomimetic cluster synthesis is based on three conceptual strategies (96,97): (i) *self-assembly*--self-organizing synthesis of clusters from simple mononuclear metal precursors and ligand reagents (the cornerstone approach for cluster synthesis); (ii) *fragment condensation*--coupling of pre-existing di- or polynuclear clusters or a cluster with a mononuclear reactant to give higher-nuclearity clusters of (in theory) predictable structures; (iii) *core conversion*--reorganization of a pre-existing cluster to a different core geometry by means of redox reactions, changes in ligand set, or reaction with an external reagent, usually a ligand nucleophile. All have proven useful in biomimetic research; (i) and (iii) are illustrated below.

Heterometal cubane-type clusters with $[MFe_3S_4]^z$ cores, including those with M = Mo and V, have been prepared by procedures (i) and (ii) (97). A sequence of reactions has been devised based on these single cubane clusters leading to the all-ferrous edge-bridged double cubanes **59** (98). The clusters, which are attractive precursors because of their high nuclearity, undergo core conversion upon reaction with hydrosulfide in acetonitrile to afford the clusters **60** (99, 100). These clusters feature a prominent μ_6-S interior atom, an overall connectivity pattern identical to **56**, and map closely upon the native P-cluster with rms deviations in atom positions of 0.33-0.38 Å (97). The clusters **60** are first topological analogues of the P-cluster. They are not chemical models because of the presence of heterometals and μ_2-S rather than thiolate bridges. Earlier, the same topology had been achieved in larger and less tractable clusters in which P-type units were connected by sulfide bridges (101,102).

An exceptional result has been obtained by cluster self-assembly in a system containing an Fe^{II} precursor with strongly basic ligands, two thiols which when deprotonated function as exceptionally capacious ligands, and elemental sulfur in toluene (Figure 19) (103). Product cluster **61** (28% yield) was isolated; it was also obtained in an assembly system not requiring prior isolation of the dinuclear intermediate. A second cluster with $(Me_3Si)_2N$ in a doubly bridging position was formed in slight amount. The toluene solvent promotes the formation of a neutral cluster in a redox-buffered reaction system containing oxidant (sulfur) and reductants (Fe^{II}, thiolate) which generates a product with $5Fe^{II} + 3Fe^{III}$. Remarkably, **61** manifests the FeMoco topology but with μ_2-SR/R* bridges rather than sulfide and sulfide rather than X as the interstitial atom. In addition to achieving the desired topology, the results demonstrate for the first time the formation of an iron-sulfur cluster with an atom interstitial to a trigonal prismatic Fe_6 cage. Taken together, clusters **60** and **61** and the methods affording them presage continued progress toward the goal of accurate synthetic analogues of the P-cluster and FeMoco.

Prospects

A perspective on biomimetic research of metallosites as presented here is offered by an earlier commentary from this laboratory (96). “Traditionally, synthetic inorganic chemistry has provided the molecular intuition needed to interpret metal behavior in biological systems. Today, in a reversal of circumstance, metallobiomolecules are posing fundamental inorganic questions whose answers lie outside our existing knowledge. It is a fitting symmetry that the relationship between inorganic chemistry and biology has come full circle. Equally important, these [synthetic] efforts have also contributed broadly to basic areas of inorganic chemistry that would probably not have been examined otherwise; the intrinsic value of such exploration should not be underestimated.” Given the progress thus far and the growing sophistication of biomimetic methodologies, it may be anticipated that the unachieved structural analogues of the polynuclear sites set out here will be realized. The value of analogues as *structural* guides or determinants (Figure 1) is diminishing as the power and productivity of crystallography and spectroscopic methods flourish.

Two additional aspects of research in this field continue apace. One is the daunting challenge of analogue systems capable of enzymatic transformations using chemical apparatus as faithful to native catalysts as possible. While an operative pathway can be won only from an enzyme itself, interrogation of analogue systems can show what is possible, among which may be the actual mechanism. It remains to be learned whether diverse functional analogues operative outside of a protein and suitable for disclosure of mechanistic information can be created. Another aspect is synthesis. While experimental protocol may not be the same, the intent differs not at all from the total synthesis of organic natural products and its contribution to biosynthetic pathways. Such work is intended not only to reach targets but also may contribute to the broad and developing area of biosynthesis of metallocenters (104) by showing what synthetic routes are feasible in the absence, and possibly in the presence, of proteins. Problems in metallocenter assembly, whether *in vivo* or by chemical synthesis, are at the forefront of contemporary metallobiochemistry. One need look no further than the current state of understanding of the biosynthetic pathway of FeMoco (105,106) for an inspiring example.

References

1. Holm RH, Solomon EI. Preface: Biomimetic Inorganic Chemistry. Chem Rev 2004;104:347–348. [PubMed: 14871127]
2. Holm RH, Solomon EI. Biomimetic Inorganic Chemistry. Chem Rev 2004;104(no 2)
3. Kraatz, HB.; Metzler-Nolte, N., editors. Concepts and Models in Bioinorganic Chemistry. Wiley-VCH; New York: 2006.
4. Hille R. The Mononuclear Molybdenum Enzymes. Chem Rev 1996;96:2757–2816. [PubMed: 11848841]
5. Schindelin H, Kisker C, Rajagopalan KV. Molybdopterin from Molybdenum and Tungsten Enzymes. Adv Protein Chem 2001;58:47–94. [PubMed: 11665493]
6. Hille R. Structure and Function of Xanthine Oxidoreductase. Eur J Inorg Chem 2006:1913–1926.
7. Schwarz G, Mendel RR. Molybdenum Cofactor Biosynthesis and Molybdenum Enzymes. Annu Rev Plant Biol 2006;57:623–647. [PubMed: 16669776]
8. Li HK, Temple C, Rajagopalan KV, Schindelin H. The 1.3 Å Crystal Structure of *Rhodobacter sphaeroides* Dimethylsulfoxide Reductase Reveals Two Distinct Molybdenum Coordination Environments. J Am Chem Soc 2000;122:7673–7680.
9. Dias JM, Than ME, Humm A, Huber R, Bourenkov GP, Bartunik HD, Bursakov S, Calvete J, Caldeira J, Carneiro C, Moura JJG, Moura I, Romão MJ. Crystal Structure of the First Dissimilatory Nitrate Reductase at 1.9 Å Solved by MAD Methods. Structure 1999;7:65–79. [PubMed: 10368307]
10. Jormakka M, Törnroth S, Byrne B, Iwata S. Molecular Basis of Proton Motive Force Generation: Structure of Formate Dehydrogenase-N. Science 2002;295:1863–1868. [PubMed: 11884747]

11. Boyington JC, Gladyshev VN, Khangulov SV, Stadtman TC, Sun PD. Crystal Structure of Formate Dehydrogenase H: Catalysis Involving Mo, Molybdopterin, Selenocysteine, and an Fe_4S_4 Cluster. Science 1997;275:1305–1308. [PubMed: 9036855]
12. Seiffert G, Ullman GM, Messerschmidt A, Schinck B, Kroneck PHM, Einsle O. Structure of the Non-redox-active Tungsten/[4Fe:4S] Enzyme Acetylene Hydratase. Proc Natl Acad Sci USA 2007;104:3073–3077. [PubMed: 17360611]
13. Raaijmakers H, Macieira S, Dias JM, Texeira S, Bursakov S, Huber R, Moura JJG, Moura I, Romão MJ. Gene Sequence and the 1.8 Å Crystal Structure of the Tungsten-Containing Formate Dehydrogenase from *Desulfovibrio gigas*. Structure 2002;10:1261–1272. [PubMed: 12220497]
14. Kisker C, Schindelin H, Pacheco A, Wehbi WA, Garrett RM, Rajagopalan KV, Enemark JH, Rees DC. Molecular Basis of Sulfite Oxidase Deficiency from the Structure of Sulfite Oxidase. Cell 1997;91:973–983. [PubMed: 9428520]
15. Schrader N, Fischer K, Theis K, Mendel RR, Schwarz G, Kisker C. The Crystal Structure of Plant Sulfite Oxidase Provides Insights into Sulfite Oxidation in Plants and Animals. Structure 2003;11:1251–1263. [PubMed: 14527393]
16. Bonin I, Martins BM, Purvanov V, Fetzner S, Huber R, Dobbek H. Active Site Geometry and Substrate Recognition of the Molybdenum Hydroxylase Quinoline 2-Oxidoreductase. Structure 2004;12:1425–1435. [PubMed: 15296736]
17. Pauff JM, Zhang J, Bell CE, Hille R. Crystal Structure of Enzyme in Reaction with 2-Hydroxy-6-methylpurine. J Biol Chem 2008;283:4818–4824. [PubMed: 18063585]
18. Kirk ML, McNaughton RL, Helton ME. The Electronic Structure and Spectroscopy of Metallo-Dithiolene Complexes. Prog Inorg Chem 2004;52:111–212.
19. Young, CG. Biomimetic Oxidations Catalyzed by Transition Metal Complexes. Meunier, B., editor. World Scientific Publishing Co.; Singapore: 2000. p. 415-459.
20. Enemark JH, Cooney JJA, Wang JJ, Holm RH. Synthetic Analogues and Reaction Systems Relevant to the Molybdenum and Tungsten Oxotransferases. Chem Rev 2004;104:1175–1200. [PubMed: 14871153]
21. Kail BW, Pérez LM, Zaric SD, Millar AJ, Young CG, Hall MB, Basu P. Mechanistic Investigation of the Oxygen-Atom-Transfer Reactivity of Dioxo-molybdenum(VI) Complexes. Chem Eur J 2006;12:7501–7509.
22. Xiao Z, Bruck MA, Enemark JH, Young CG, Wedd AG. A Catalytic Cycle Related to Molybdenum Enzymes Containing $[Mo^{VI}O_2]^{2+}$ Oxidized Active Sites. Inorg Chem 1996;35:7508–7515.
23. Doonan CJ, Rubie ND, Peariso K, Harris HH, Knottenbelt SZ, George GN, Young CG, Kirk ML. Electronic Description of the *cis*-MoOS Unit in Models for Molybdenum Hydroxylases. J Am Chem Soc 2008;130:55–65. [PubMed: 18062689]
24. Schultz BE, Gheller SF, Muetterties MC, Scott MJ, Holm RH. Molybdenum-Mediated Oxygen Atom Transfer: An Improved Analogue Reaction System of the Molybdenum Oxotransferases. J Am Chem Soc 1993;115:2714–2722.
25. Jiang J, Holm RH. An Expanded Set of Functional Groups in Bis(dithiolene)tungsten(IV,VI) Complexes Related to the Active Sites of Tungstoenzymes, Including W^{IV}-SR and W^{VI}-O(SR). Inorg Chem 2004;43:1302–1310. [PubMed: 14966965]
26. Wang JJ, Kryatova O, Rybak-Akimova EV, Holm RH. Comparative Kinetics and Mechanism of Oxygen and Sulfur Atom Transfer Reactions Mediated by Bis(dithiolene) Complexes of Molybdenum and Tungsten. Inorg Chem 2004;43:8092–8101. [PubMed: 15578849]
27. Jiang J, Holm RH. Reaction Systems Related to Dissimilatory Nitrate Reductase: Nitrate Reduction Mediated by Bis(dithiolene)tungsten Complexes. Inorg Chem 2005;44:1068–1072. [PubMed: 15859288]
28. Wang JJ, Tessier C, Holm RH. Analogue Reaction Systems of Selenate Reductase. Inorg Chem 2006;45:2979–2988. [PubMed: 16562954]
29. Bertero MG, Rothery RA, Palak M, Hou C, Lim D, Blasco F, Weiner JH, Strynadka NCJ. Insights into the Respiratory Electron Transfer Pathway from the Structure of Nitrate Reductase A. Nature Struct Biol 2003;10:681–687. [PubMed: 12910261]

30. Raaijmakers HCA, Romão MJ. Formate-reduced *E. coli* Formate Dehydrogenase H: the Reinterpretation of the Crystal Structure Suggests a New Reaction Mechanism. J Biol Inorg Chem 2006;11:849–854. [PubMed: 16830149]

31. Lim BS, Willer MW, Miao M, Holm RH. Monodithiolene Molybdenum(V,VI) Complexes: A Structural Analogue of the Oxidized Active Site of the Sulfite Oxidase Enzyme Family. J Am Chem Soc 2001;123:8343–8349. [PubMed: 11516283]

32. Groysman S, Wang JJ, Tagore R, Lee SC, Holm RH. A Biomimetic Approach to Oxidized Sites in the Xanthine Oxidoreductase Family: Synthesis and Stereochemistry of Tungsten(VI) Analogue Complexes. J Am Chem Soc 2008;130:12794–12807. [PubMed: 18763763]

33. Sung KM, Holm RH. Oxo Transfer Reactions Mediated by Bis(dithiolene)tungsten Analogues of the Active Sites of Molybdoenzymes in the DMSO Reductase Family: Comparative Reactivity of Tungsten and Molybdenum. J Am Chem Soc 2001;123:1931–1943. [PubMed: 11456814]

34. Majumdar A, Pal K, Sarkar S. Selectivity of Thiolate Ligand and Preference of Substrate in Model Reactions of Dissimilatory Nitrate Reductase. Inorg Chem 2008;47:3393–3401. [PubMed: 18335980]

35. Sugimoto H, Tarumizu M, Miyake H, Tsukube H. Bis(dithiolene) Molybdenum Complex that Promotes Combined Coupled Electron-Proton Transfer and Oxygen Atom Transfer Reactions: A Water-Active Model of the Arsenite Oxidase Molybdenum Center. Eur J Inorg Chem 2008:4494–4497.

36. Lubitz W, van Gastel M, Gaertner W. Nickel Iron Hydrogenases. Met Ions Life Sci 2007;2:279–322.

37. Fontecilla-Camps JC, Volbeda A, Cavazza C, Nicolet Y. Structure-Function Relationships of the [NiFe]- and [FeFe]-Hydrogenase. Chem Rev 2007;107:4273–4303. [PubMed: 17850165]

38. Lemon, BJ.; Peters, JW. Handbook of Metalloproteins. Wiley & Sons Ltd.; Chichester, U.K.: 2001. p. 738-751.

39. Nicolet Y, Cavazza C, Fontecilla-Camps JC. Fe-only Hydrogenases: Structure, Function, and Evolution. J Inorg Biochem 2002;91:1–8. [PubMed: 12121756]

40. Shima S, Pilak O, Vogt S, Schick M, Stagni MS, Meyer-Klaucke W, Warkentin E, Thauer RK, Ermler U. The Crystal Structure of [Fe]-Hydrogenase Reveals the Geometry of the Active Site. Science 2008;321:572–575. [PubMed: 18653896]

41. Georgakaki, IP.; Darensbourg, MY. Bio-coordination Chemistry. Que, L., Jr; Tolman, WA., editors. Elsevier; Oxford: 2004. p. 549-568.

42. Bouwman E, Reedijk J. Structural and Functional Models Related to the Nickel Hydrogenases. Coord Chem Rev 2005;249:1555–1581.

43. Liu X, Ibrahim SK, Tard C, Pickett CJ. Iron-only Hydrogenase: Synthetic, Structural, and Reactivity Studies of Model Compounds. Coord Chem Rev 2005;249:1641–1652.

44. van der Vlugt JI, Meyer F. Synthetic Models for the Active Sites of Nickel-Containing Enzymes. Met Ions Life Sci 2007;2:181–240.

45. Canaguier S, Artero V, Fontecave M. Modelling NiFe Hydrogenases: Nickel-Based Electrocatalysts for Hydrogen Production. Dalton Trans 2008:315–325. [PubMed: 18411840]

46. Volbeda A, Fontecilla-Camps JC. Structural Bases for the Catalytic Mechanism of Ni-containing Carbon Monoxide Dehydrogenases. J, Chem Soc, Dalton Trans 2005:3443–3450.

47. Volbeda A, Martin L, Cavazza C, Matho M, Faber BW, Roseboom W, Albracht SPJ, Garcin E, Rousset M, Fontecilla-Camps JC. Structural Differences Between the Ready and Unready Oxidized States of [NiFe] Hydrogenases. J Biol Inorg Chem 2005;10:239–249. [PubMed: 15803334]

48. Ogata H, Hirota S, Nakahara A, Komori H, Shibata N, Kato T, Kano K, Higuchi Y. Process of [NiFe] Hydrogenase Eludicidated by High-Resolution X-Ray Analysis: Conversion of the Ready to the Unready State. Structure 2005;13:1635–1642. [PubMed: 16271886]

49. Garcin E, Vernede X, Hatchikian EC, Volbeda A, Frey M, Fontecilla-Camps JC. The Crystal Structure of a Reduced [NiFeSe] Hydrogenase Provides an Image of the Activated Catalytic Center. Structure 1999;7:557–566. [PubMed: 10378275]

50. Sellman D, Geipel F, Heinemann FW. $(NEt_4)[Fe(CN)_2(CO)(‘S3’)]$: An Iron Thiolate Complex Modeling the $[Fe(CN)_2(CO)(S\text{-}Cys)_2]$ Site of the [NiFe] Hydrogenase Centers. Chem Eur J 2002;8:958–966.

51. James TL, Cai L, Muetterties MC, Holm RH. Dihydrogen Evolution by Protonation Reactions of Nickel(I). Inorg Chem 1996;35:4148–4161. [PubMed: 11666623]
52. Sellman D, Geipel F, Moll M. [Ni(NHPPr$^{n}_{3}$)('S3')], the First Nickel Thiolate Complex Modeling the Nickel Cysteinate Site and Reactivity of [NiFe] Hydrogenase. Angew Chem Int Ed Engl 2000;39:561–563. [PubMed: 10671258]
53. Li Z, Ohki Y, Tatsumi K. Dithiolato-Bridged Dinuclear Iron-Nickel Complexes [$Fe(CO)_2(CN)_2$(μ-$SCH_2CH_2CH_2S$)Ni(S_2CNR_2)]$^-$ Modeling the Active Site of [NiFe] Hydrogenases. J Am Chem Soc 2005;127:8950–8951. [PubMed: 15969562]
54. Ohki Y, Yasamura K, Kuge K, Tanino S, Ando M, Li Z, Tatsumi K. Thiolate-bridged Dinuclear Iron (tris-carbonyl)-nickel Complexes Relevant to the Active Site of [NiFe] Hydrogenase. Proc Natl Acad Sci USA 2008;105:7652–7657. [PubMed: 18511566]
55. Ogo S, Kabe R, Uehara K, Kure B, Nishimura T, Menon SC, Harada R, Fukuzumi S, Higuchi Y, Ohhara T, Tamada T, Kuroki R. A Dinuclear Ni(μ-H)Ru Complex Derived from H_2. Science 2007;316:585–587. [PubMed: 17463285]
56. Pandey AS, Harris TV, Giles LJ, Peters JW, Szilagyi RK. Dithiomethylether as a Ligand in the Hydrogenase H-Cluster. J Am Chem Soc 2008;130:4533–4540. [PubMed: 18324814]
57. Seyferth D, Henderson RS, Song LC. The Dithiobis(tricarbonyliron) Dianion: Improved Preparation and New Chemistry. J Organometal Chem 1980;192:C1–C5.
58. Singleton ML, Bhuvanesh N, Reibenspies JH, Darensbourg MY. Synthetic Support of De Novo Design: Sterically Bulky [FeFe]-Hydrogenase Models. Angew Chem Int Ed 2008;47:9492–9495.
59. Stack TDP, Holm RH. Subsite-Differentiated Analogues of Biological [4Fe-4S]$^{2+}$ Clusters: Synthesis, Solution and Solid State Structures, and Subsite-Specific Reactions. J Am Chem Soc 1988;110:2484–2494.
60. Tard C, Liu X, Ibrahim SK, Bruschi M, De Giola L, Davies SC, Yang X, Wang LS, Sawers G, Pickett CJ. Synthesis of the H-cluster Framework of Iron-only Hydrogenase. Nature 2005;433:610–613. [PubMed: 15703741]
61. Capon JF, Gloaguen F, Schollhammer P, Talarmin J. Catalysis of Electrochemical H_2 Evolution by Di-iron Subsite Models. Coord Chem Rev 2005;249:1664–1676.
62. Heiden ZM, Zampella G, De Gioia L, Rauchfuss TB. [FeFe]-Hydrogenase Models and Hydrogen: Oxidative Addition of Dihydrogen and Silanes. Angew Chem Int Ed 2008;47:9756–9759.
63. Beinert H, Holm RH, Münck E. Iron-Sulfur Clusters: Nature's Modular, Multipurpose Structures. Science 1997;277:653–659. [PubMed: 9235882]
64. Johnson DC, Dean DR, Smith AD, Johnson MK. Structure, Function, and Formation of Biological Iron-Sulfur Clusters. Annu Rev Biochem 2005;74:247–281. [PubMed: 15952888]
65. Morales R, Chron MH, Hudry-Clergeon G, Pétillot Y, Norager S, Medina M, Frey M. Refined X-ray Structures of Oxidized, at 1.3 Å, and Reduced, at 1.17 Å, [2Fe-2S] Ferredoxin from the Cyanobacterium *Anabaena* PCC7119 Show Redox-Linked Conformational Changes. Biochemistry 1999;38:15764–15773. [PubMed: 10625442]
66. Bönisch H, Schmidt CL, Schäfer G, Ladenstein R. The Structure of the Soluble Domain of an Archaeal Rieske Iron-Sulfur Protein at 1.1 Å Resolution. J Mol Biol 2002;319:791–805. [PubMed: 12054871]
67. Nielsen MS, Harris P, Ooi BL, Christensen HEM. The 1.5 Å Resolution Crystal Structure of [Fe_3S_4]-Ferredoxin from the Hyperthermophilic Archaeon *Pyrococcus furiosus*. Biochemistry 2004;43:5188–5194. [PubMed: 15122884]
68. Fukuyama K, Okada T, Kakuta Y, Takahashi Y. Atomic Resolution Structures of Oxidized [4Fe-4S] Ferredoxin from *Bacillus thermoproteolyticus* in Two Crystal Forms: Systematic Distortion of [4Fe-4S] Cluster in the Protein. J Mol Biol 2002;315:1155–1166. [PubMed: 11827483]
69. Rao PV, Holm RH. Synthetic Analogues of the Active Sites of Iron-Sulfur Proteins. Chem Rev 2004;104:527–559. [PubMed: 14871134]
70. Holm, RH. Electron Transfer: Iron-Sulfur Clusters. In: Que, L., Jr; Tolman, WA., editors. Bio-coordination Chemistry. Elsevier; Oxford: 2004. p. 61-90.
71. Link TA. The Structures of Rieske and Rieske-Type Proteins. Adv Inorg Chem 1999;47:83–157.
72. Ballmann J, Albers A, Demeshko S, Dechert S, Bill E, Bothe E, Ryde U, Meyer F. A Synthetic Analogue of Rieske-Type [2Fe-2S] Clusters. Angew Chem Int Ed 2008;47:9537–9541.

73. Brown EN, Friemann R, Karlsson A, Parales JV, Couture MMJ, Eltis LD, Ramaswany S. Determining the Rieske Cluster Reduction Potentials. J Biol Inorg Chem 2008;13:1301–1313. [PubMed: 18719951]
74. Yoo SJ, Angove HC, Burgess BK, Hendrich MP, Münck E. Mössbauer and Integer-Spin EPR Studies and Spin-Coupling Analysis of the [4Fe-4S]^0 Cluster of the Fe Protein of *Azotobacter vinelandii* Nitrogenase. J Am Chem Soc 1999;121:2534–2545.
75. Strop P, Takahara PM, Chiu HJ, Angove HC, Burgess BK, Rees DC. Crystal Structure of the All-Ferrous [4Fe-4S]^0 Form of the Nitrogenase Iron Protein from *Azotobacter vinelandii*. Biochemistry 2001;40:651–656. [PubMed: 11170381]
76. Scott TA, Berlinguette CP, Holm RH, Zhou HC. Initial Synthesis and Structure of an All-Ferrous Analogue of the Fully Reduced [Fe_4S_4]^0 Cluster of the Nitrogenase Iron Protein. Proc Natl Acad Sci USA 2005;102:9741–9744. [PubMed: 15985547]
77. Deng L, Holm RH. Stabilization of Fully Reduced Iron-Sulfur Clusters by Carbene Ligation: The [Fe_nS_n]^0 Oxidation Levels (n = 4, 8). J Am Chem Soc 2008;130:9878–9886. [PubMed: 18593124]
78. Chakrabarti M, Deng L, Holm RH, Münck E, Bominaar EL. Mössbauer, Electron Paramagnetic Resonance and Theoretical Study of a Carbene-Based All-Ferrous Fe_4S_4 Cluster: Electronic Origin and Structural Identification of the Unique Spectroscopic Site. Inorg Chem. 2009in press
79. Dobbek H, Gremer L, Meyer O, Huber R. Crystal Structure and Mechanism of CO Dehydrogenase: aMolybdo Iron-Sulfur Flavoprotein Containing *S*-selanylcysteine. Proc Natl Acad Sci USA 1999;96:8884–8889. [PubMed: 10430865]
80. Ragsdale SW, Kumar M. Nickel-Containing Carbon Monoxide Dehydrogenase/Acetyl-CoA Synthase. Chem Rev 1996;96:2515–2539. [PubMed: 11848835]
81. Lindahl PA, Graham DE. Acetyl-coenzyme A Synthases and Nickel-Containing Carbon Monoxide Dehydrogenases. Metal Ions Life Sci 2007;2:357–415.
82. Lindahl PA. Implications of a Carboxylate-Bound C-Cluster Structure of Carbon Monoxide Dehydrogenase. Angew Chem Int Ed 2008;47:4054–4056.
83. Dobbek H, Gremer L, Kiefersauer R, Huber R, Meyer O. Catalysis at a Dinuclear [CuSMo(=O)OH] Cluster in a CO Dehydrogenase Resolved at 1.1-Å Resolution. Proc Natl Acad Sci USA 2002;99:15971–15976. [PubMed: 12475995]
84. Gourley C, Nielsen DJ, White JM, Knottenbelt SZ, Kirk ML, Young CG. Paramagnetic Active Site Models for the Molybdenum-Copper Carbon Monoxide Dehydrogenase. J Am Chem Soc 2006;128:2164–2165. [PubMed: 16478141]
85. Takuma M, Ohki Y, Tatsumi K. Sulfido-Bridged Dinuclear Molybdenum-Copper Complexes Related to the Active Site of CO Dehydrogenase: [(dithiolate)Mo(O)S_2Cu(SAr)]$^{2-}$ (dithiolate = 1,2-$S_2C_6H_4$, 1,2-$S_2C_6H_2$-3,6-Cl_2, 1,2-$S_2C_2H_4$). Inorg Chem 2005;44:6034–6043. [PubMed: 16097823]
86. Zhou J, Raebiger JW, Crawford CA, Holm RH. Metal Ion Incorporation Reactions of the Cluster [Fe_3S_4(LS_3)]$^{3-}$, Containing the Cuboidal [Fe_3S_4]^0 Core. J Am Chem Soc 1997;119:6242–6250.
87. Panda R, Berlinguette CP, Zhang Y, Holm RH. Synthesis of MFe_3S_4 Clusters Containing a Planar M^{II} Site (M = Ni, Pd, Pt), a Structural Element in the C-Cluster of Carbon Monoxide Dehydrogenase. J Am Chem Soc 2005;127:11092–11101. [PubMed: 16076217]
88. Sun J, Tessier C, Holm RH. Sulfur Ligand Substitution at the Nickel(II) Sites of Cubane-Type and Cubanoid NiFe_3S_4 Clusters Relevant to the C-Clusters of Carbon Monoxide Dehydrogenase. Inorg Chem 2007;46:2691–2699. [PubMed: 17346040]
89. Dobbek H, Svetlitchnyi V, Liss J, Meyer O. Carbon Monoxide Induced Decomposition of the Active Site [Ni-4Fe-5S] Cluster of CO Dehydrogenase. J Am Chem Soc 2004;126:5382–5387. [PubMed: 15113209]
90. Jeoung JH, Dobbek H. Carbon Dioxide Activation at the Ni,Fe-Cluster of Anaerobic Carbon Monoxide Dehydrogenase. Science 2007;318:1461–1464. [PubMed: 18048691]
91. Howard JB, Rees DC. Structural Basis of Biological Nitrogen Fixation. Chem Rev 1996;96:2965–2982. [PubMed: 11848848]
92. Howard JB, Rees DC. How Many Metals Does It Take to Fix N_2? A Mechanistic Overview of Biological Nitrogen Fixation. Proc Natl Acad Sci USA 2006;103:17088–17093. [PubMed: 17088547]

93. Peters JW, Stowell MHB, Soltis SM, Finnegan MG, Johnson MK, Rees DC. Redox-Dependent Structural Changes in the Nitrogenase P-Cluster. Biochemistry 1997;36:1181–1187. [PubMed: 9063865]

94. Mayer SM, Lawson DM, Gormal CA, Roe SM, Smith BE. New Insights into Structure-function Relationships in Nitrogenase: A 1.6 Å X-ray Crystallographic Study of *Klebsiella pneumoniae* MoFe-protein. J Mol Biol 1999;292:871–891. [PubMed: 10525412]

95. Einsle O, Tezcan FA, Andrade SLA, Schmid B, Yoshida M, Howard JB, Rees DC. Nitrogenase MoFe-Protein at 1.16 Å Resolution: A Central Ligand in the FeMo-Cofactor. Science 2002;297:1696–1700. [PubMed: 12215645]

96. Lee SC, Holm RH. Speculative Synthetic Chemistry and the Nitrogenase Problem. Proc Natl Acad Sci USA 2003;100:3595–3600. [PubMed: 12642670]

97. Lee SC, Holm RH. The Clusters of Nitrogenase: Synthetic Methodology in the Construction of Weak-Field Clusters. Chem Rev 2004;104:1135–1157. [PubMed: 14871151]

98. Berlinguette CP, Miyaji T, Zhang Y, Holm RH. Precursors to Clusters with the Topology of the P^N Cluster of Nitrogenase: Edge-Bridged Double Cubane Clusters $[(Tp)_2Mo_2Fe_6S_8L_4]^z$ -- Synthesis, Structures, and Electron Transfer Series. Inorg Chem 2006;45:1997–2007. [PubMed: 16499360]

99. Zhang Y, Holm RH. Synthesis of a Molecular $Mo_2Fe_6S_9$ Cluster with the Topology of the P^N Cluster of Nitrogenase by Rearrangement of an Edge-Bridged $Mo_2Fe_6S_8$ Double Cubane. J Am Chem Soc 2003;125:3910–3920. [PubMed: 12656626]

100. Zuo JL, Zhou HC, Holm RH. Vanadium-Iron-Sulfur Clusters Containing the Cubane-Type $[VFe_3S_4]$ Core Unit: Synthesis of a Cluster with the Topology of the P^N Cluster of Nitrogenase. Inorg Chem 2003:4624–4631. [PubMed: 12870953]

101. Osterloh F, Sanakis Y, Staples RJ, Münck E, Holm RH. A Molybdenum-Iron-Sulfur Cluster Containing Structural Elements Relevant to the P-Cluster of Nitrogenase. Angew Chem Int Ed 1999;38:2066–2070.

102. Osterloh F, Achim C, Holm RH. Reduced Molybdenum-Iron-Sulfur Clusters of Nuclearities Eight and Sixteen, Including a Topological Analogue of the P-Cluster of Nitrogenase. Inorg Chem 2001;40:224–232. [PubMed: 11170527]

103. Ohki Y, Ikagawa Y, Tatsumi K. Synthesis of New [8Fe-7S] Clusters: A Topological Link between the Core Structures of P-Cluster, FeMo-co and FeFe-co of Nitrogenase. J Am Chem Soc 2007;129:10457–10465. [PubMed: 17676736]

104. Kukchar J, Hausinger RP. Biosynthesis of Metal Sites. Chem Rev 2004;104:509–525. [PubMed: 14871133]

105. Dos Santos PC, Dean DR, Hu Y, Ribbe MW. Formation and Insertion of the Nitrogenase Iron-Molybdenum Cofactor. Chem Rev 2004;104:1159–1173. [PubMed: 14871152]

106. Hu Y, Fay AW, Lee CC, Yoshizawa J, Ribbe MW. Assembly of Nitrogenase MoFe protein. Biochemistry 2008;47:3973–3981. [PubMed: 18314963]

Abbreviations (see also Figure 3)

CODH
carbon monoxide dehydrogenase

DMSOR
dimethylsulfoxide reductase

FDH
formate dehydrogenase

FeMoco
iron-molybdenum cofactor

FTIR
Fourier transform infrared

Im
: imidazole

L
: ligand (generalized)

M
: metal (generalized)

Me_3tacn
: *N*,*N*′,*N*″-trimethyl-1,4,7-triazacyclononane

NiR
: nitrate reductase

Q
: oxygen, sulfur, selenium

S_2-*o*-xyl
: *o*-xylyl-α,α'-dithiolate(2-)

S_2pd
: pyranopterindithiolate(2-)

SO
: sulfite oxidase

XOR
: xanthine oxidoreductase

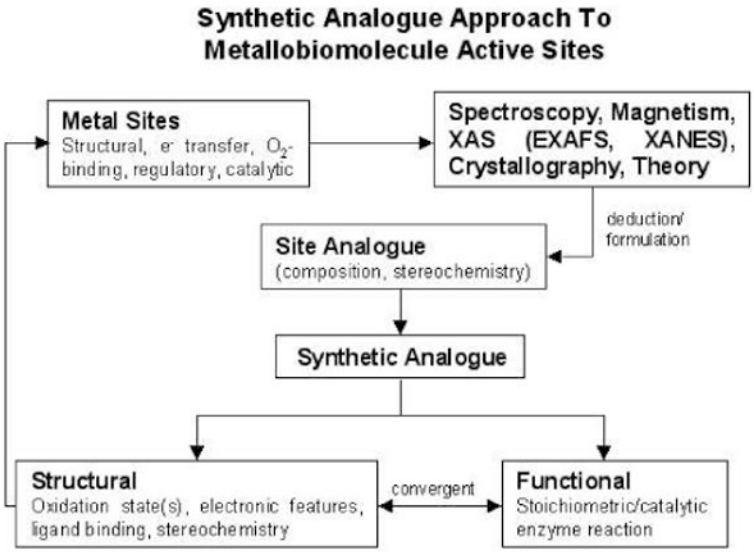

Figure 1.
Schematic representation of the synthetic analogue approach to metallobiomolecule active sites. The arrow on the left signifies repetition of the process leading to an improved analogue.

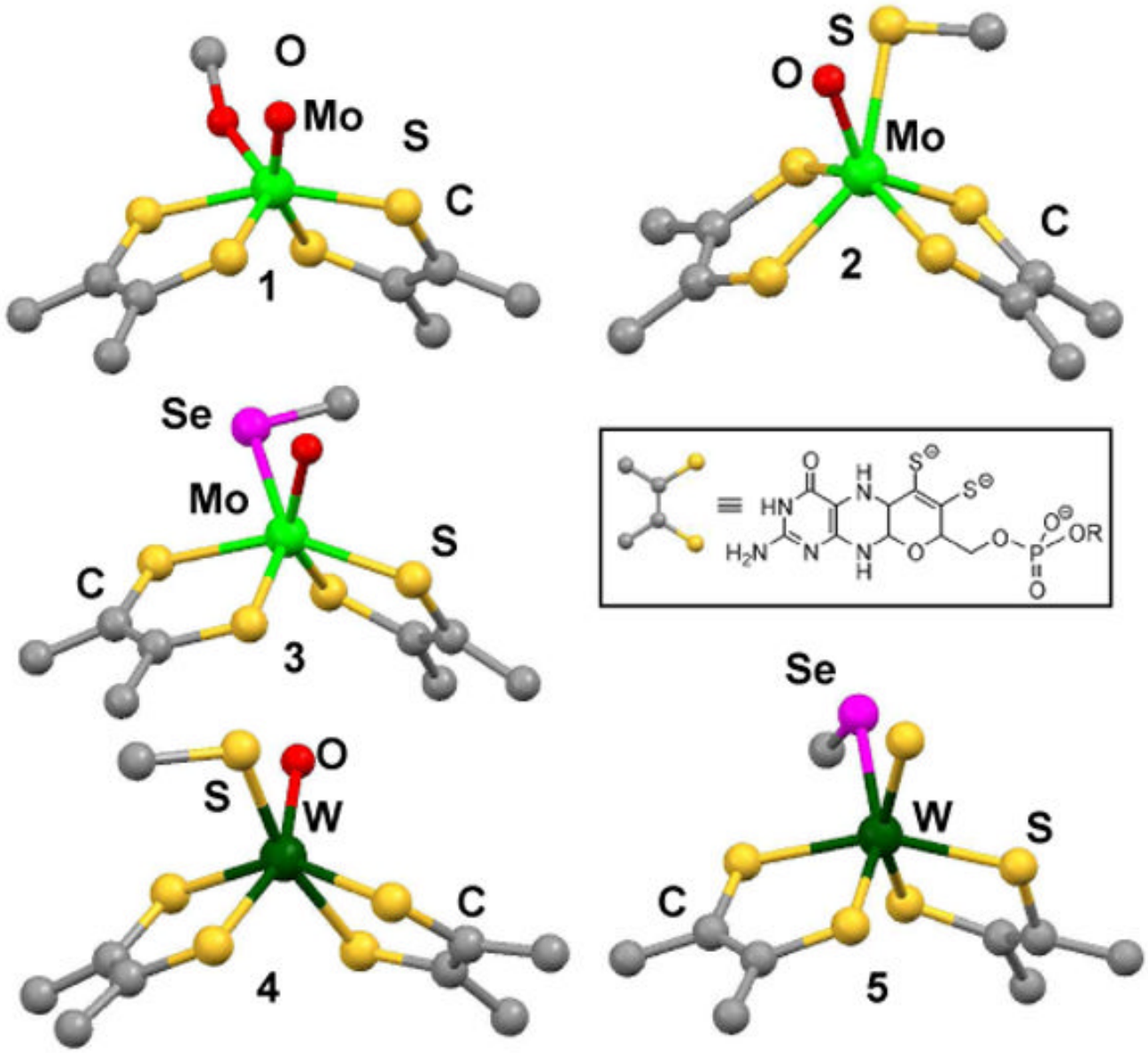

Figure 2.

Oxidized active site structures in the molybdoenzyme DMSOR family: **1**, DMSO reductase (*R. sphaeroides*, 1.3 Å resolution, PDB code 1EU1, one conformation) (8); **2**, dissimilatory nitrate reductase (*D. desulfuricans*, 1.9 Å resolution, PDB code 2NAP) (9); **3**, formate dehydrogenase N (*E. coli*, 1.6 Å resolution, PDB code 1KQF) (10). Tungsten enzymes: **4**, acetylene hydratase (*P. acetylenicus*, 1.26 Å resolution, PDB code 2E7Z) (12); **5**: formate dehydrogenase (*D. gigas*, 1.8 Å resolution, PDB code 1H0H) (13). The pyranopterindithiolate cofactor ligand is depicted in the box (R = nucleotide).

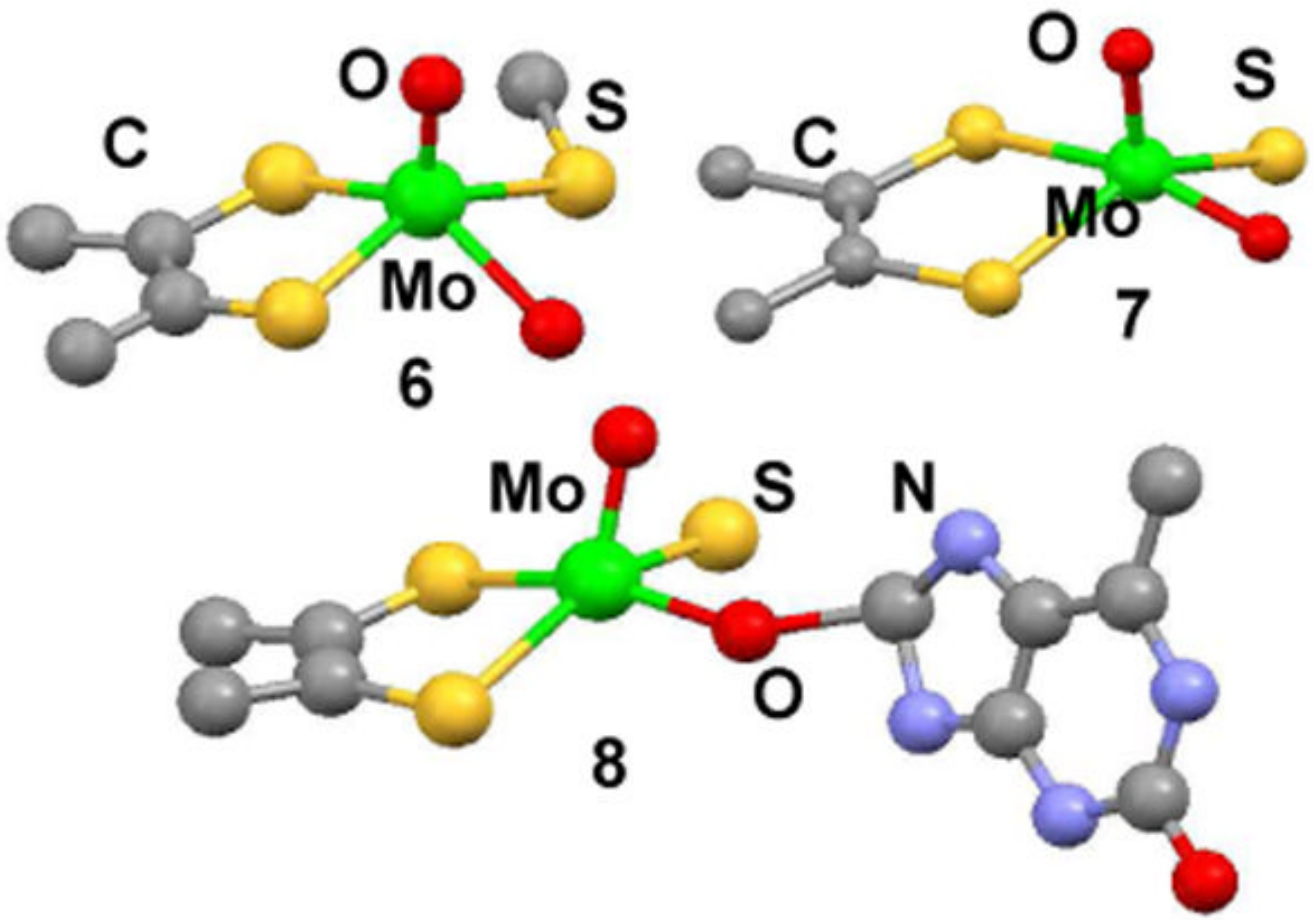

Figure 3.
Oxidized active site structures in the molybdoenzyme SO and XOR families: **6**, sulfite oxidase (chicken liver, 1.9 Å, PDB code 1SOX) (14); **7**, quinoline-2-oxidoreductase (*P. putida*, 1.8 Å resolution, PDB code 1T3Q) (16); **8**, reaction intermediate of xanthine oxidoreductase and 2-hydroxy-6-methylpurine, 2.3 Å, PDB code 3B9J) (17)

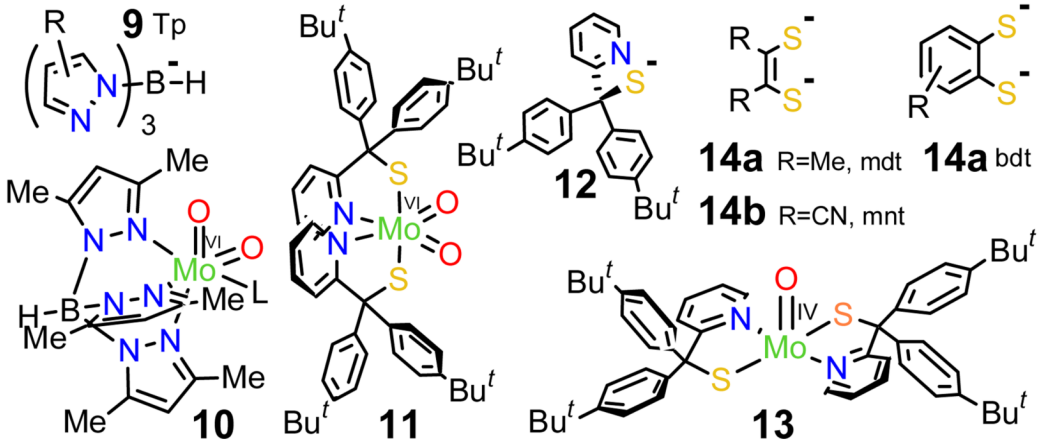

Figure 4.
Ligands and complexes in biomimetic molybdenum/tungsten chemistry: tridentate hydrotris (pyrazolyl)borate(1-) **9** and an $Mo^{VI}O_2$ complex **10** (L variable), bidentate 2-pyridyldiphenylmethanethiolate(1-) (**11**) and its sterically encumbered $Mo^{VI}O_2$ (**12**) and $Mo^{IV}O$ (**13**) complexes, and dithiolate ligands **14**.

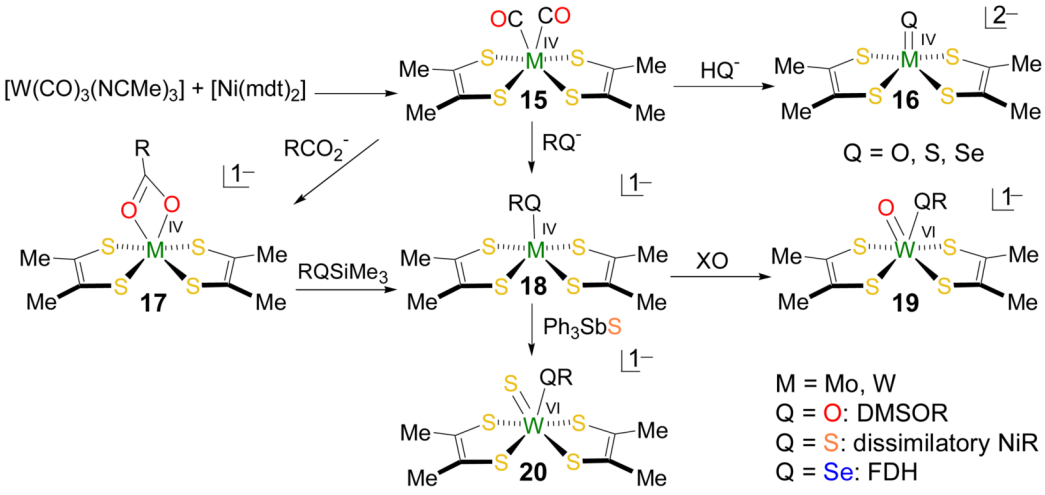

Figure 5.

Synthesis of unprotonated analogues of reduced (**17, 18**) and oxidized (**19**) active sites of three members of the DMSOR family (M = Mo; Q = O, S, Se). Complex **20** is an analogue of the oxidized site in W-FDH. Reduced analogues have square pyramidal structures and oxidized analogues and **17** adopt six-coordinate structures distorted toward trigonal prismatic geometry.

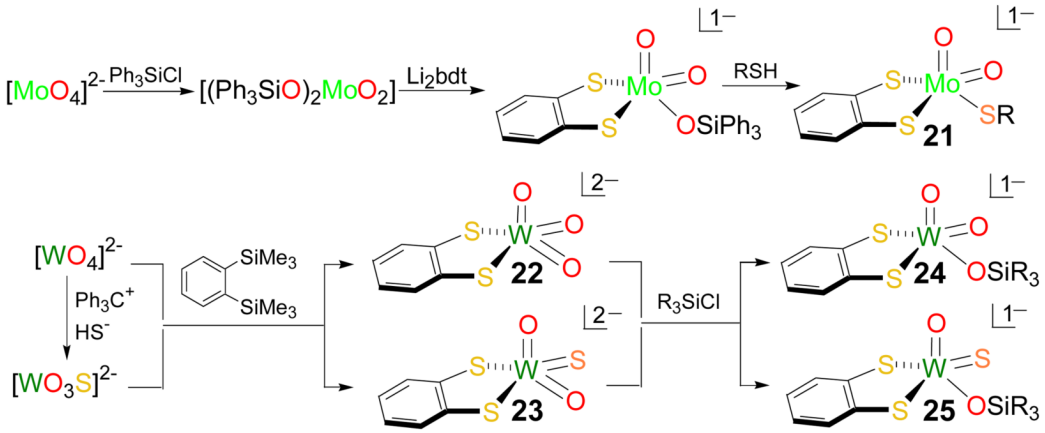

Figure 6.
Synthetic schemes leading to structural analogues of the active sites of members of the SO (**21**) and XOR (**23**) families. Complex **22** represents an inactive site and **24** and **25** monoprotonated inactive and active sites, respectively, in the XOR family.

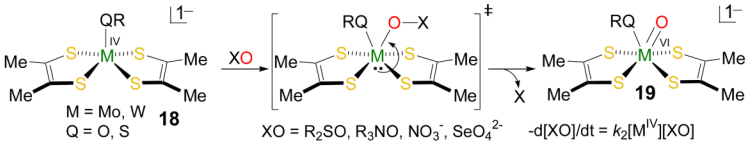

Figure 7.
Schematic representation of functional reductase analogue reaction systems for *S*-oxides, *N*-oxides, nitrate, and selenate.

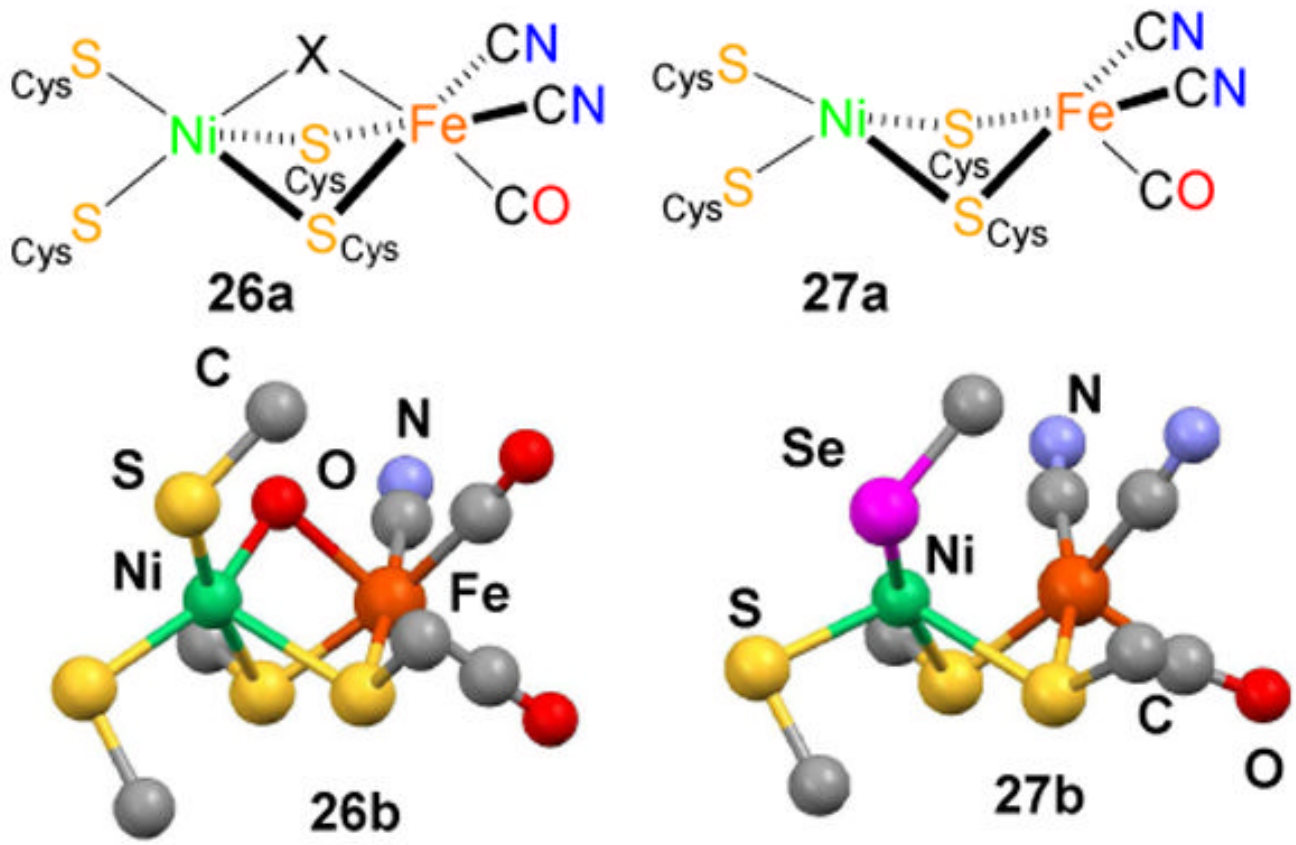

Figure 8.

Representative hydrogenase active site structures: oxidized [NiFe] (**26a**) and a specific example (**26b**, *D. vulgaris*, 1.4 Å resolution, PDB code 1WUJ) (48); reduced [NiFe] (**27a**) and a specific example of reduced [NiFeSe] (**27b**, *D. maculatum*, 2.15 Å resolution, PDB code 1CC1) (49)

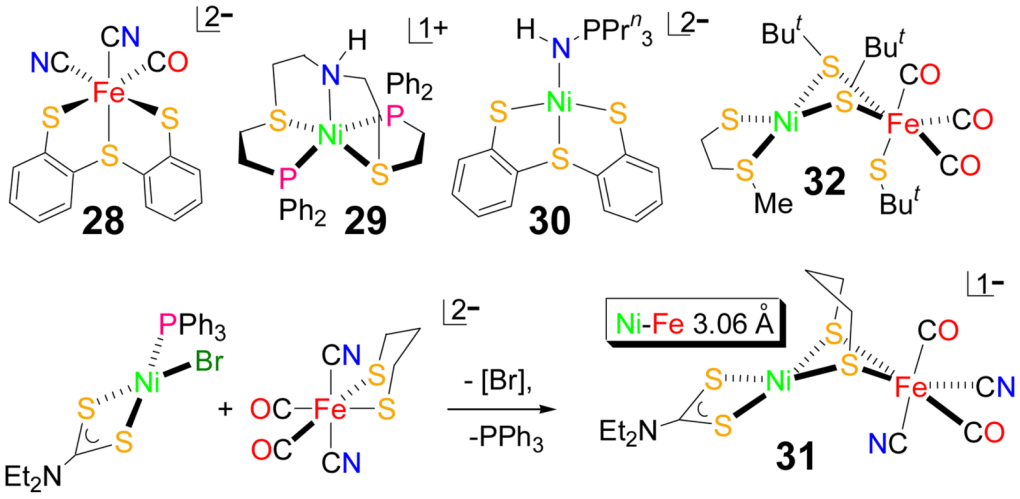

Figure 9.
Mononuclear complexes **28-30** and NiFe complex **32**, and preparation of NiFe complex **31**.

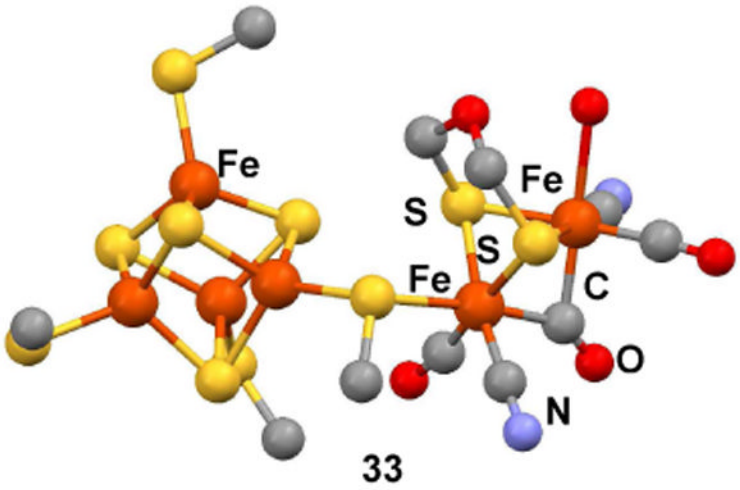

Figure 10.
Structure of the H-cluster of an [FeFe] hydrogenase in the oxidized active form (**33**, *C. pasteurianum*, 1.4 Å resolution, PDB code 3C8Y) (56). In the dinuclear fragment, the carbonyl bridge is slightly asymmetric (Fe-C 1.91, 1.96 Å) and the Fe-Fe distance (2.55 Å) is consistent with direct metal-metal interaction.

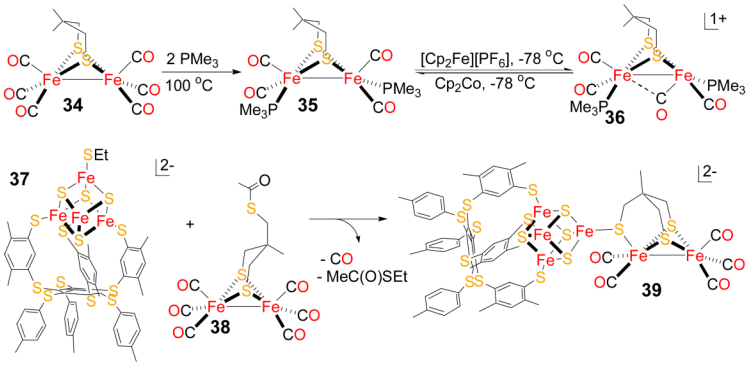

Figure 11.
Reactions leading to a models of the dinuclear fragment (**36**) and the entire framework (**39**) of the H-cluster.

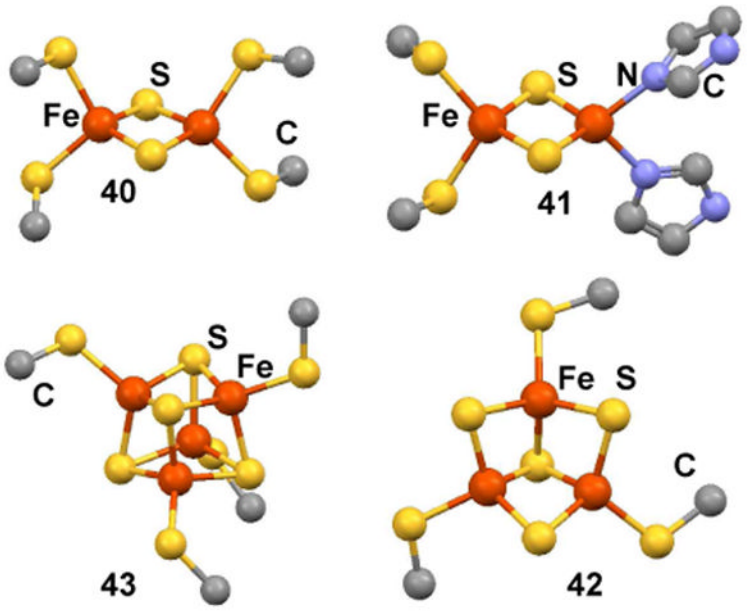

Figure 12.
Structures of the clusters $\{Fe_2S_2(S_{Cys})_4\}$ (**40**, *Anabaena*, 1.2-1.3 Å resolution, PDB code 1CZP) (65), $\{Fe_2S_2(S_{Cys})_2(N_{His})_2\}$ (**41**, *S. acidocaldarius*, 1.1 Å resolution, PDB code 1JM1) (66), $\{Fe_3S_4(S_{Cys})_3\}$ (**42**, *P. furious*, 1.5 Å resolution, PDB code 1SJ1) (67), and $\{Fe_4S_4(S_{Cys})_4\}$ (**43**, *B. thermoproteolyticus*, 0.9-1.0 Å resolution, PDB code 1IQZ) (68).

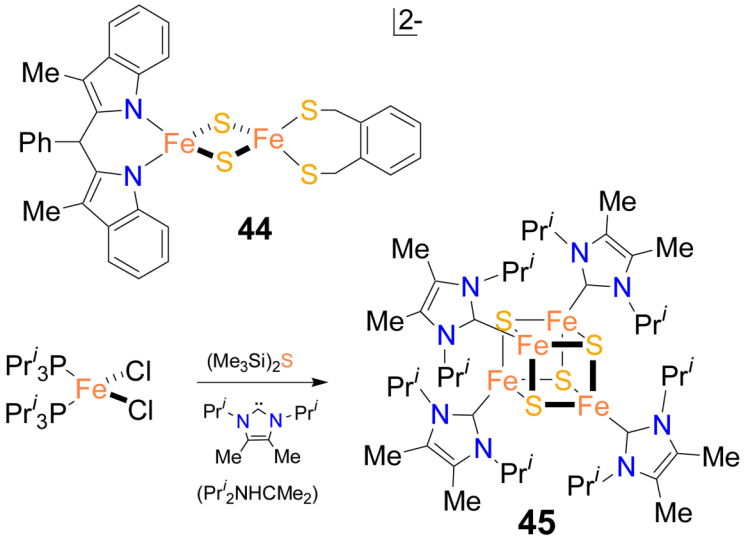

Figure 13.

The oxidized Rieske cluster analogue **44** and the preparation of all-ferrous analogue **45** of the fully reduced cluster in the Fe protein of nitrogenase.

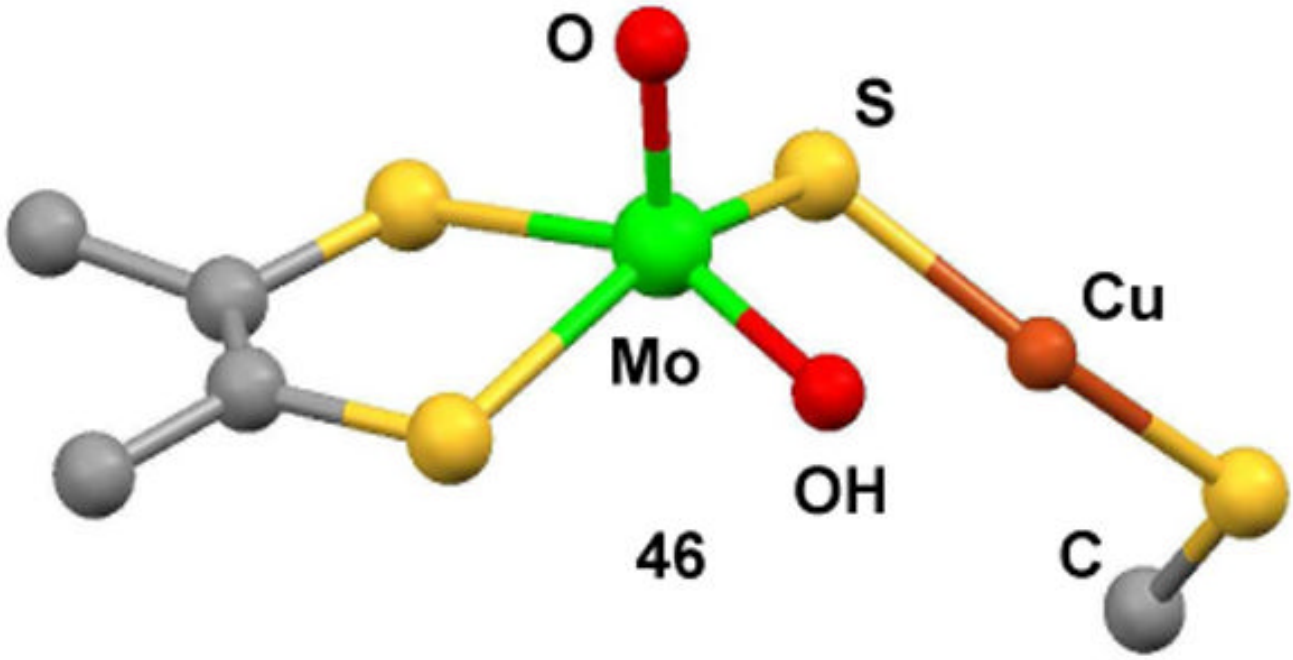

Figure 14.

Oxidized active site structure of Cu-Mo CODH (**46**, *O. carboxidovorans*, 1.1 Å resolution, PDB code 1N5W) (83); Cu···Mo 3.74 Å, Mo-S 2.27 Å, Cu-S 2.21 Å, Cu-S_{Cys} 2.22 Å, Mo-S-Cu 113°, S-Cu-S 156°. The reduced site (Mo^{IV}/Cu^{I}) has the same structure with small differences in parameters except for the Mo-S-Cu angle and the Mo···Cu distance which increase by about 10° and 0.5 Å, respectively.

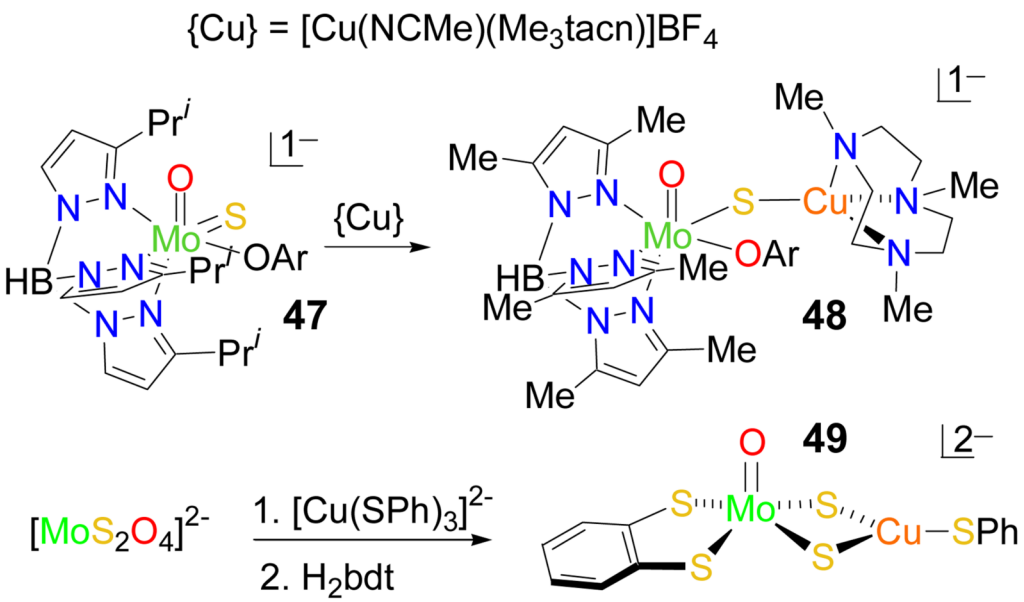

Figure 15.
Synthetic routes to bridged complexes **48** and **49** having certain structural elements in common with Mo-Cu CODH site **46**.

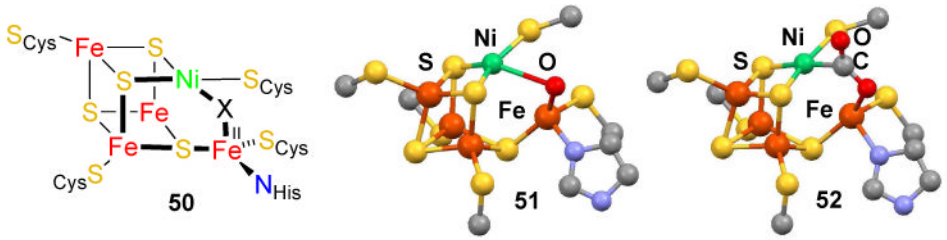

Figure 16.
Generalized structure **50** of the Ni-Fe CODH sites **51** and **52** (*C. hydrogenoformans*, 1.4-1.5 Å resolution, PDB code 3B52) (90).

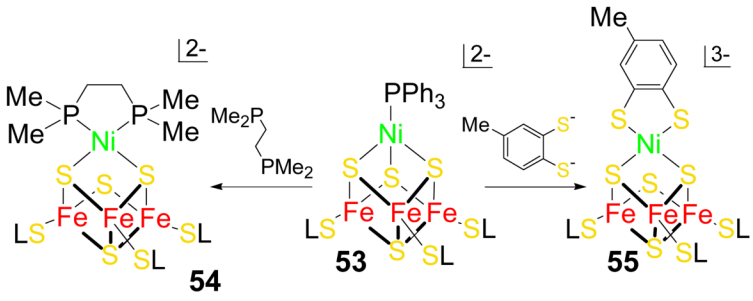

Figure 17.
Synthesis of cubanoid clusters **54** and **55** by ligand substitution of **53**. The 3 LS notation refers to the tridentate thiolate ligand in cluster **37** (Figure 11).

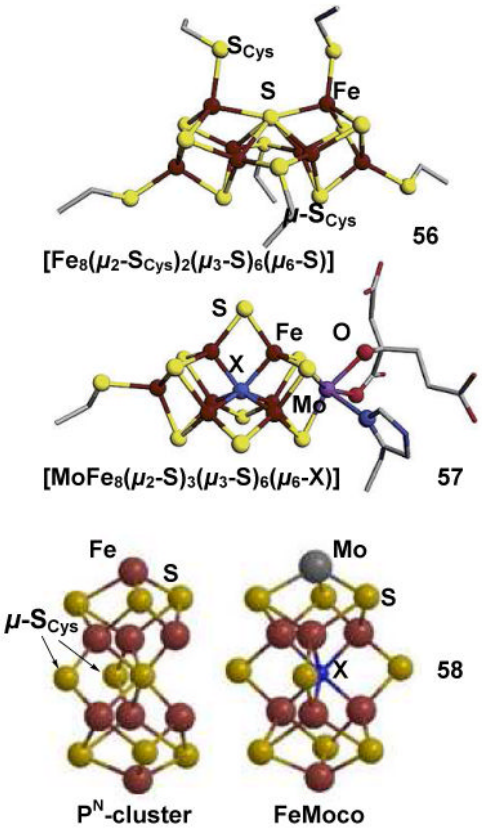

Figure 18.

Structures of the P-cluster **56** and FeMoco **57** (*A. vinelandii* MoFe protein; 2.0 and 1.2 Å resolution; PDB codes 2MIN, 1M1N) of nitrogenase (93,95) and a comparison **58** of cluster topologies.

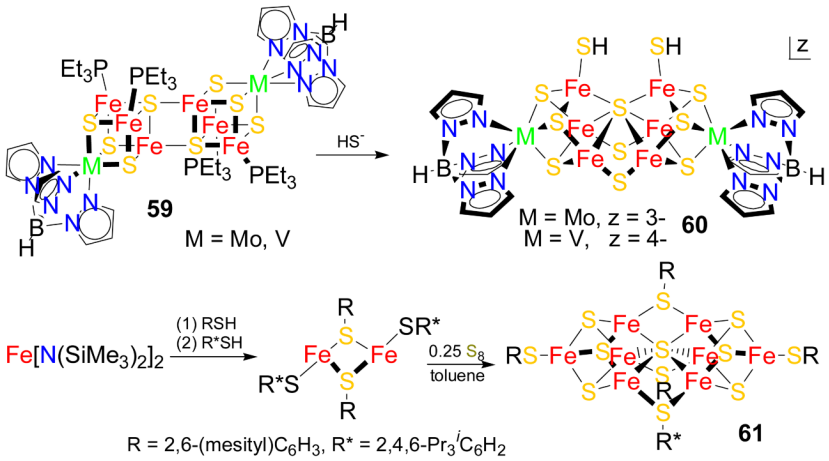

Figure 19.

Synthetic reactions affording topological analogues of the P-cluster (**60**) and cofactor cluster (**61**) of nitrogenase.